RSC Advances

PAPER

View Article Online
View Journal | View Issue

Cite this: *RSC Adv.*, 2017, **7**, 39824

One-step preparation of TiO_2 particles with controllable phase and morphology by plasma electrolysis

Chenxu Liu,[ab] Qian Zhao,[a] Linxiu Wang,[b] Jin Zhang,*[b] Yu Tian[a] and Yonggang Meng *[a]

TiO_2 particles were prepared by plasma electrolysis with a one-step method in aqueous solution. By adjusting the $Ti(SO_4)_2$ concentration, the phase and morphology of the synthesized particles were well controlled. When $Ti(SO_4)_2$ concentration was in the range of 0.1–0.3 mol L^{-1}, TiO_2 particles with anatase as the main phase were obtained. From transmission electron microscopy (TEM) and inverse fast Fourier transform (FFT) analysis results, the average grain size of the particles was found to be about 4.0–6.0 nm, which was in accordance with X-ray diffraction (XRD) results. Micrographs showed that the surface of the particles obtained in the low concentrations was rough and composed of tiny nano-structures (about 10 nm). With increase of the concentration, the main phase of the TiO_2 particles was transformed from anatase to rutile and the grain size became bigger, while particle size became smaller and the surface of the particles was smoother. When the concentration was higher than 0.6 mol L^{-1}, TiO_2 particles with rutile as the main phase were synthesized. The average grain size of the anatase increased to 30.0–50.0 nm, and the rutile's size was about 60.0–75.0 nm. By measuring the current density–time curves, the effect of concentration on phase and morphology of the particles has been explained. The function of the cathode material and the generation of TiO_2 particles have also been discussed, after analyzing the compositions, microstructure and weight of cathode material before and after plasma electrolysis.

Received 19th June 2017
Accepted 10th August 2017

DOI: 10.1039/c7ra06840a

rsc.li/rsc-advances

1. Introduction

As one of the most popular semiconductor materials, titanium oxide (TiO_2) plays a pivotal role in numerous fields, due to its special features in optical, electrical and thermal stability.[1,2] Anatase and rutile are the most frequently encountered polymorphic phases of TiO_2. The anatase structure TiO_2 (anatase-TiO_2) has huge potential application value in photovoltaic cells,[3–6] owing to its superior electron mobility and slightly larger band gap. A majority of studies on anatase materials have focused on synthetic materials in the forms of powders and thin films. Rutile is the stable phase, whereas anatase is metastable and tends to transform into rutile upon heating.[7,8] The rutile structure TiO_2 (rutile-TiO_2) has even more applications, such as a photocatalytic material, white pigment, in cosmetics and as an electrode material for lithium-ion batteries.[9–11] In addition, the mixed phase structures have been researched for some new properties and synergetic effects due to the interface lattice mismatch between the two phases.[7]

In order to further improve the properties of the TiO_2 and broaden the fields of its application, preparation of TiO_2 with nano/micro structure has been received considerable attention especially in recent years. Many methods have been proposed for the synthesis of special structured TiO_2, such as hydrothermal method,[12–15] hydrolysis method,[10,16,17] mechanochemical synthesis,[18,19] chemical vapor synthesis[20] and sol–gel method.[21] A common feature of these methods is multistep process, generally including a treatment at high temperature for several hours. Thus, it is easy to cause agglomeration and instability of the nano/micro structure.

Plasma electrolysis technology is a hybrid of traditional electrolysis and atmospheric plasma process. Owing to its efficient work and low requirements of equipment, plasma electrolysis has received more and more attention in the field of coating preparation and surface treatment.[22–25] There are still a few studies focusing on synthesis of microspheres and particles by using this novel method. Guo *et al.* have synthesized Al_2O_3 and TiO_2 microspheres respectively by using NH_4NO_3 aqueous solution as the electrolyte, Al and Ti as the cathode materials.[26,27] Anis Allagui *et al.* have prepared Ni, NiO or Pt nanomaterials with cathode contact glow discharge electrolysis

[a]*State Key Laboratory of Tribology, Tsinghua University, Beijing 100084, China. E-mail: mengyg@tsinghua.edu.cn*

[b]*Beijing Key Laboratory for Corrosion Erosion and Surface Technology, Institute of Advanced Materials and Technology, University of Science and Technology Beijing, Beijing 100083, China. E-mail: zhangjin@ustb.edu.cn*

in acidic and alkaline media by alternating the Ni and Pt cathode.[28,29] Tomohiro Akiyama *et al.* have synthesized Sn/SnO_2 nanoparticles *via* surfactant-free direct-current electrolysis using KCl as the electrolyte and metallic Sn wire as the cathode.[30] The nano/microspheres prepared in all of these researches are formed by a 'melting-quenching' process of the cathode materials. Owing to this reason, the microspheres are greatly influenced by the cathode materials. The surface of some microspheres is metal oxide by oxidation, while the interior is still metal, which greatly affects the quality and the purity of microspheres. What's more, the production rate is very low.

Recently, we firstly used the metal ions in salt solution as the source of ceramic microspheres, instead of the cathode material. Thus, Al_2O_3 microspheres have been successfully prepared by plasma electrolysis in an aqueous solution of $Al(NO)_3$.[31] What's more, because compositions of microspheres can be well controlled by the compositions of salt solutions, $La_2Zr_2O_7$ microspheres have been also directly prepared by this method in the mixed electrolyte of $Zr(NO_3)_4$ and $La(NO_3)_3$.[32] Hopefully, this novel method is considered as a favorable and simple way to attain much more kinds of microspheres in salt solutions at room temperature.

In this study, plasma electrolysis has been further developed and TiO_2 particles have been successfully prepared in $Ti(SO_4)_2$ solutions in only one step. By adjusting the concentration of the solutions, phases and morphologies of the particles have been well controlled. These phenomena have been analyzed by exploring the mechanism of plasma electrolysis. By measuring the current density–time curves, the effect of concentration on phase and morphology of the particles has been explained. The function of the cathode material and the generation of TiO_2 particles have also been discussed, after analyzing the compositions, microstructure and weight of cathode material before and after plasma electrolysis.

2. Experimental

Preparation of TiO_2 particles

TiO_2 particles were prepared by a one-step plasma electrolysis method. A schematic diagram of plasma electrolysis device was shown in Fig. 1a. A platinum electrode worked as anode with a dimension of 120 mm × 50 mm × 0.3 mm. The sample of Ti alloy (6.3% Al, 4.2% V, 0.15% O, 0.11% Fe, 0.03% C, 0.02% N, 0.001% H, balance Ti, wt%) after polishing was used as cathode material, owing to its stable physical and chemical properties. The dimension of the cathode material was 15 mm × 10 mm × 2 mm, much smaller than the anode to ensure formation of plasma on the cathode surface. Aqueous solutions consisted of $Ti(SO_4)_2$ and polyethylene glycol (25 g L^{-1}). Concentrations of the $Ti(SO_4)_2$ were 0.1 mol L^{-1}, 0.2 mol L^{-1}, 0.3 mol L^{-1}, 0.4 mol L^{-1}, 0.6 mol L^{-1} and 0.8 mol L^{-1}, also denoted hereafter as 0.1 M, 0.2 M, 0.3 M, 0.4 M, 0.6 M and 0.8 M respectively.

A pulsed electrical power supply (TN-KGZ01) was connected to the electrolytic bath. Evolutions of voltage with time in different solutions were measured with a computer installed with an AD data acquisition card. The applied voltage was

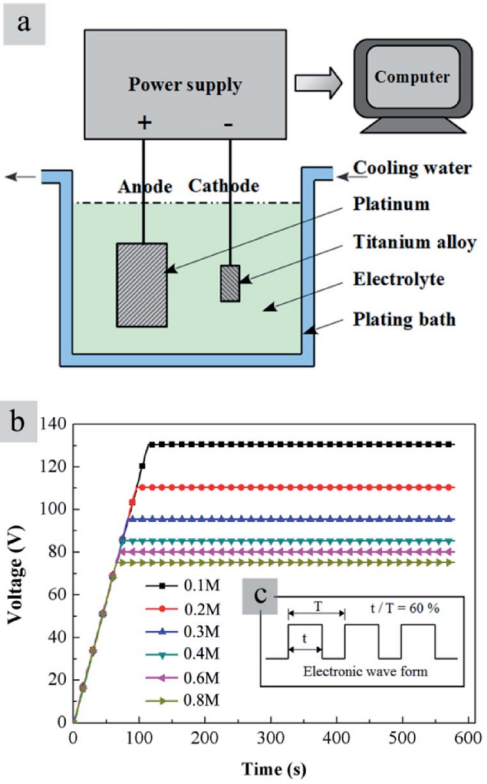

Fig. 1 (a) Schematic diagram of the plasma electrolysis device; (b) voltage–time curves in $Ti(SO_4)_2$ solutions with different concentrations and (c) wave form of the pulsed electrical power supply.

increased at the rate of 1 V s^{-1} and held at a fixed value for about 500 s to prepare particles. For the $Ti(SO_4)_2$ solutions with different concentrations, the voltage values for the stabilized plasma electrolysis reactions were different. It was considered that when the concentration was low, the resistance of the solution was big. Thus, the plasma electrolysis process needed large potentials for stabilization of reactions. Experiments suggested that the suitable voltage value in 0.1 mol L^{-1} $Ti(SO_4)_2$ solution was 130 V, and the suitable voltage values in other solutions were different as shown in Fig. 1b. The frequency was controlled at about 500 Hz and duty ratio 60%. The wave form of the pulsed electrical power supply was shown in Fig. 1c. A thermostatic water bath was used to control the temperature of the electrolyte under 50 °C.

In the initial stage of plasma electrolysis process, cathode material in solution was covered with bubbles. Then, the voltage was increased until bright micro-arcs could be observed on the surface of cathode. As a result, the electrolyte became cloudy and particles could be obtained. After centrifugation, washing (by distilled water and ethyl alcohol) and drying, the particles were purified for characterization.

Morphological and structural characterization

Microstructure and elementary compositions of the samples were characterized by environmental scanning electron microscope (SEM and EDS, FEI QUANTA 200 FEG). High

magnification SEM micrographs of TiO_2 particles were characterized by field emission scanning electron microscope (FESEM, HITACHI SU8220) to analyze the fine structures in a single particle. Surface topography of the particles was measured by using the tapping mode of an AFM (Bruker Dimension ICON). Surface of the cathode material after the plasma electrolysis was further observed after mechanical etching by focused ion beam (FIB, FEI QUANTA 200 FEG).

Phase structures of the samples were characterized by X-ray diffraction (XRD, using a Cu Kα radiation SmartLab-3 kW, scanning from 20° to 60° for particles samples and from 10° to 90° for block samples, with step of 0.02°, scan rate 2° min^{-1}). Grain sizes and relative content of different phases were analyzed by using a program named THCLXPD (Tsinghua University, China). The high resolution electron micrographs and selected area electron diffraction (SAED) patterns of the samples were characterized by high resolution transmission electron microscopy (TEM, JEM-2100F). The original data and inverse fast Fourier transformation (FFT) were analyzed by using the software named RADIUS. Before the TEM inspection, the samples were pretreated by ultra-thin microtome (Leica, UC7+FC7, Germany) to ensure the thickness of the particle samples was less than 70 nm.

Before and after the plasma electrolysis, the mass of Ti alloy samples was weighed by the analytical balance (Mettler AE240, China) to get the weight change of the cathode materials. The evolutions of cathode current densities with time were recorded to analysis the different processes during plasma electrolysis in different concentrations of the electrolyte.

3. Results

Fig. 2 shows the effect of the solution concentrations on sample morphology. It is obvious that the particle size displays a regular change with increase of the solution concentrations. In Fig. 2a, the product prepared in 0.1 mol L^{-1} $Ti(SO_4)_2$ solution is comprised of particles with diameters in the range of 600–1200 nm. When the concentration of $Ti(SO_4)_2$ is 0.2 mol L^{-1} or 0.3 mol L^{-1}, the size of particles is about 800 ± 200 nm, as shown in Fig. 2b and c. When the concentration is 0.4 mol L^{-1}, the particle size becomes smaller, about 600 ± 200 nm, as shown in Fig. 2d. When $Ti(SO_4)_2$ concentration increases to 0.6 mol L^{-1} or 0.8 mol L^{-1}, the size of the most particles is small, about 300 ± 150 nm. However, there exists serious agglomeration. Some big particles with diameters more than 2 μm mixed in the products prepared in 0.6 mol L^{-1} and 0.8 mol L^{-1} $Ti(SO_4)_2$ solutions, in Fig. 2e and f.

To further observe more detailed morphology of a single particle, field emission scanning electron microscope (FESEM) has been used and the results are shown in Fig. 3. From the FESEM micrographs in Fig. 3a–d, some tiny structures about 10 nm can be observed on the surface of the particles prepared in 0.1–0.4 mol L^{-1} $Ti(SO_4)_2$ solutions. For the particles prepared in 0.6 and 0.8 mol L^{-1} $Ti(SO_4)_2$ solutions, showing in Fig. 3e and f, the particle size is smaller than the particles prepared in the lower concentrations and there is almost no tiny structures on the surface of particles made of these two kinds of solutions.

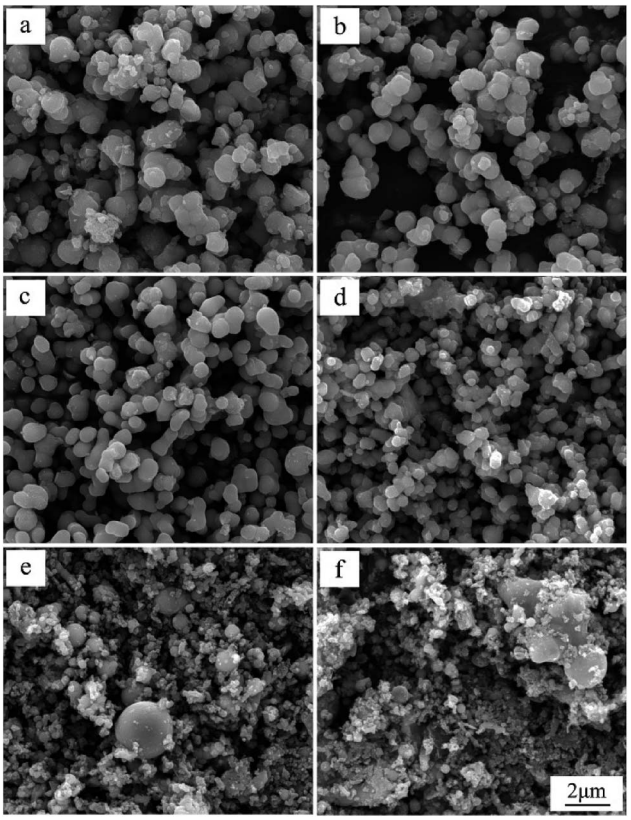

Fig. 2 SEM micrographs of particles prepared by plasma electrolysis in $Ti(SO_4)_2$ solutions with different concentrations: (a) 0.1 mol L^{-1}, (b) 0.2 mol L^{-1}, (c) 0.3 mol L^{-1}, (d) 0.4 mol L^{-1}, (e) 0.6 mol L^{-1} and (f) 0.8 mol L^{-1}.

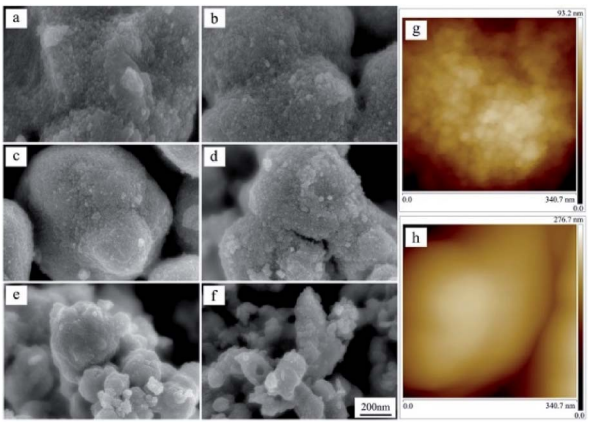

Fig. 3 High magnification FESEM micrographs of the particles prepared by plasma electrolysis in $Ti(SO_4)_2$ solutions with different concentrations: (a) 0.1 mol L^{-1}, (b) 0.2 mol L^{-1}, (c) 0.3 mol L^{-1}, (d) 0.4 mol L^{-1}, (e) 0.6 mol L^{-1} and (f) 0.8 mol L^{-1}; AFM micrographs of the particles prepared in (g) 0.3 mol L^{-1} and (h) 0.8 mol L^{-1} $Ti(SO_4)_2$ solutions.

Further more, surface topographies of particles have been also measured with an AFM. Fig. 3g and h show the AFM micrographs of particles prepared in 0.3 mol L^{-1} and 0.8 mol L^{-1} $Ti(SO_4)_2$ solutions, respectively. The results also present that the

surface of the particles prepared in the low concentration is rough and composed of tiny structures, while the surface of the particles prepared in the high concentration is relatively smooth.

Fig. 4 shows XRD patterns of the samples prepared by plasma electrolysis with different solution concentrations. When concentrations of the $Ti(SO_4)_2$ solutions are lower than 0.4 mol L^{-1} (including 0.1 mol L^{-1}, 0.2 mol L^{-1} and 0.3 mol L^{-1} in this experiment), the products are mainly composed of anatase-TiO_2 (JCPDS no. 21-1272). When the $Ti(SO_4)_2$ concentration is 0.4 mol L^{-1}, the particles consist of anatase-TiO_2 and rutile-TiO_2 (JCPDS no. 21-1276). In comparison with the anatase TiO_2, the diffraction lines of the rutile TiO_2 are obviously sharp, which suggests large grain size. With the increase of the $Ti(SO_4)_2$ concentration, peaks of the anatase-TiO_2 become weak and peaks of rutile-TiO_2 become strong. When the concentration is 0.8 mol L^{-1}, the product is mainly composed of rutile-TiO_2. In Table 1, the relative contents of rutile-TiO_2 in different samples have been quantitatively measured according to the XRD results and analyzed by the THCLXPD program (Tsinghua University, China). The results show that with the increase of the $Ti(SO_4)_2$ concentration, there is more and more rutile-TiO_2 generated. By adjusting the concentrations of $Ti(SO_4)_2$ solutions, phase proportions of the TiO_2 particles can be modulated and the relative contents of rutile-TiO_2 can be controlled from 2.60% to 72.05%.

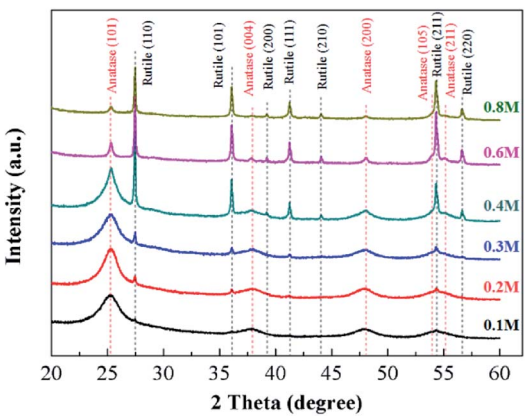

Fig. 4 XRD patterns of the particles prepared by plasma electrolysis in $Ti(SO_4)_2$ solutions with different concentrations.

Table 1 also shows grain sizes of TiO_2 particles prepared by plasma electrolysis in $Ti(SO_4)_2$ solutions with different concentrations. The average grain sizes of anatase and rutile have been determined by Scherrer's formula and analyzed by the THCLXPD program. The line width has been corrected for instrumental broadening by employing the pattern of standard-sample silicon under the same experimental conditions. In the present study, the peak broadening analysis is performed on the (101), (004), (200) reflections of anatase phase and (101), (111), (211) reflections of rutile phase, considering that the others almost superimpose with some reflections. Based on the X-ray peak broadening analysis, the average grain size of anatase in the TiO_2 particles prepared in low concentrations (0.1 mol L^{-1}, 0.2 mol L^{-1} and 0.3 mol L^{-1}) is estimated to be 4.0–6.0 nm. Owing the content in these conditions is less than 8.77%, the grain size of the rutile-TiO_2 hasn't been measured, because of the precision of the instrument and the program. At 0.4 mol L^{-1} $Ti(SO_4)_2$ solution, the average grain size of anatase TiO_2 become big, about 6.0–20.0 nm, and the content of the rutile is up to about 26.94%. The result shows that the average grain size of the rutile-TiO_2 prepared in this condition is about 70.0 nm. When the $Ti(SO_4)_2$ concentration is further increased to 0.6 mol L^{-1} and 0.8 mol L^{-1}, the average grain size of anatase TiO_2 increases to about 30.0–50.0 nm and the average grain size of the rutile-TiO_2 is about 60.0–75.0 nm.

These results clearly indicate that the $Ti(SO_4)_2$ concentration plays an important role in preparation of TiO_2 particles. With the increase of concentrations, the main phase of the TiO_2 particles is transformed from anatase to rutile. When the concentration of the $Ti(SO_4)_2$ solution is low, the content of anatase-TiO_2 is high and the average grain size small. When the concentration is high, the content of rutile-TiO_2 is high and the average grain size is big.

To verify the results of the XRD measurement, TEM images of the TiO_2 particles prepared by plasma electrolysis in 0.3 mol L^{-1} and 0.8 mol L^{-1} $Ti(SO_4)_2$ solutions have been analyzed, as shown in Fig. 5 and 6, respectively. A structure with diameter bigger than 500 nm is seen from the low-magnification image (Fig. 5a). The selected area electron diffraction (SAED) pattern in Fig. 5b shows concentric rings corresponding to the diffraction planes of the sample prepared in 0.3 mol L^{-1} $Ti(SO_4)_2$ solution. The values of *d*-spacing of the diffraction planes are calculated and compared with those of

Table 1 Mean grain sizes of TiO_2 particles prepared by plasma electrolysis in $Ti(SO_4)_2$ solutions with different concentrations and relative contents of rutile-TiO_2

Concentration of $Ti(SO_4)_2$	Grain size (nm)						Relative contents of rutile-TiO_2
	A(101)	A(004)	A(200)	R(101)	R(111)	R(211)	
0.1 M	4.1 ± 0.4	4.0 ± 0.2	4.7 ± 0.2	—	—	—	2.60%
0.2 M	5.4 ± 0.1	5.6 ± 0.3	5.4 ± 0.8	—	—	—	4.92%
0.3 M	5.9 ± 0.5	4.2 ± 0.6	4.9 ± 0.1	—	—	—	8.77%
0.4 M	9.2 ± 1.8	19.0 ± 0.8	6.6 ± 0.6	72.2 ± 1.0	68.1 ± 7.8	62.8 ± 1.5	26.94%
0.6 M	30.2 ± 2.4	32.2 ± 2.2	24.8 ± 0.3	74.1 ± 1.7	64.9 ± 2.9	61.8 ± 1.2	70.40%
0.8 M	33.5 ± 3.6	45.9 ± 9.3	33.9 ± 1.9	75.5 ± 0.9	70.2 ± 3.9	69.5 ± 3.2	72.05%

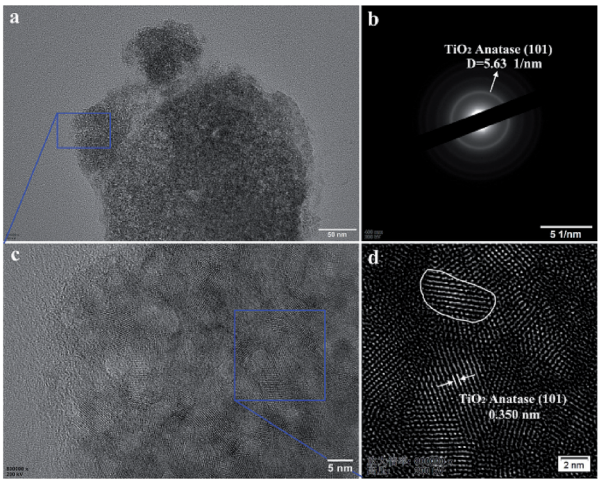

Fig. 5 (a) TEM image of TiO_2 particles prepared by plasma electrolysis in 0.3 mol L^{-1} $Ti(SO_4)_2$ solution; (b) SAED pattern; (c) HRTEM image and (d) the inverse FFT image generated from the selected area in (c).

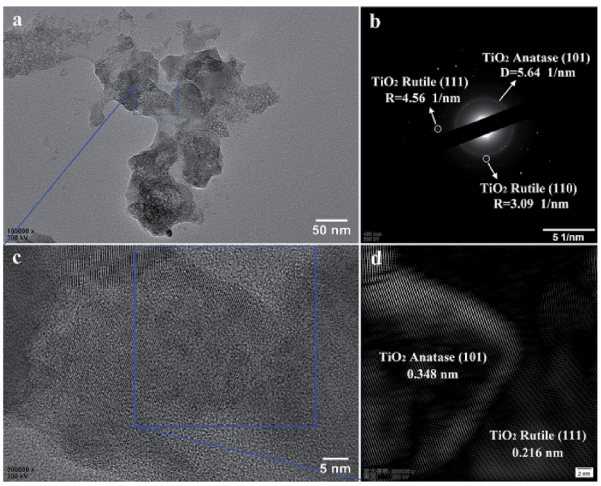

Fig. 6 (a) TEM image of TiO_2 particles prepared by plasma electrolysis in 0.8 mol L^{-1} $Ti(SO_4)_2$ solution; (b) SAED patterns; (c) HRTEM image and (d) the inverse FFT image generated from the selected area in (c).

the JCPDS standard. It is found that the diffraction pattern corresponds to TiO_2 with anatase structure, agreed well with the results from XRD measurement. A closer inspection (Fig. 5c) of the Fig. 5a reveals that the structure is an aggregate of a large number of crystalline grains. From the inverse fast Fourier transform (FFT) image (Fig. 5d) taken from a portion of Fig. 5c, we can see that the lattice spacing is about 0.350 nm, very close to that of the lattice spacing of anatase-TiO_2 (101) plane. What's more, the grain size of the nano-crystalline shown by TEM image and the inverse FFT image is about 5.0 nm in diameter. By using the XRD spectra and Scherrer formula, calculated grain sizes of the particles prepared in 0.3 mol L^{-1} $Ti(SO_4)_2$ solution are about 4.0–6.0 nm, as shown in Table 1. The calculated values are in accord with those determined from the TEM images.

In Fig. 6, TEM images of the TiO_2 particles prepared by plasma electrolysis in 0.8 mol L^{-1} $Ti(SO_4)_2$ solution have also been analyzed. The results show that though the particle size is smaller than that prepared in 0.3 mol L^{-1} $Ti(SO_4)_2$ solution (compare Fig. 5a and 6a), the grain size is bigger (compare Fig. 5c and 6c). The SAED pattern in Fig. 6b is acquired to confirm the crystalline phases of the particles. The result shows the particles consist of anatase-TiO_2 and rutile-TiO_2, also agreed well with the XRD detection. In Fig. 6d, the inverse FFT image taken from a portion of Fig. 6c shows the lattice spacing of about 0.348 nm and 0.216 nm, very close to the lattice spacings of anatase-TiO_2 (101) plane and rutile-TiO_2 (111) plane, respectively. The grain size of the nano-crystalline shown by TEM image and the inverse FFT image is about 30–70 nm in diameter much bigger than the grain size shown in Fig. 5. These results are also supported by the XRD results.

4. Discussion

Considering that plasma electrolysis is a new method to prepare TiO_2 particles, it is important to further elucidate the formation processes of the reaction product. In our previous studies, the mechanisms of plasma electrolysis for Al_2O_3 and $La_2Zr_2O_7$ microspheres preparation in nitrate aqueous solutions have been discussed.[31,32] It is considered that there are three steps for the microsphere formation. Firstly, metal ion turns into metal hydroxide in the cathode reaction; then, plasma energizes the intermediate to metallic oxide; finally, the majority of the metallic oxide turned into the coating on the cathode, and the other part formed suspending microspheres under the effect of the surface tension in the electrolyte. Thus, the essential difference between this plasma electrolysis and other "melting-quenching" processes of the cathode material[26–30] has been clarified to some extent.

For the formation mechanism of TiO_2 particles by plasma electrolysis, although the basic processes are considered to be almost similar to that of Al_2O_3 and $La_2Zr_2O_7$ microspheres, there are still some differences. For example, an Al_2O_3 or $La_2Zr_2O_7$ coating is deposited on the cathode when the microspheres are synthesized, while there is no obvious coating deposited during the preparation of TiO_2 particles. Under this condition, the formation mechanism of the TiO_2 particles needs to be further explored, involving the following three aspects: (1) the generation processes of TiO_2 particles; (2) the quantitative analysis of the effect of the $Ti(SO_4)_2$ concentrations on phase and morphology of the products; (3) the function of the cathode material and why the $Ti(SO_4)_2$ concentration is the main factor.

Let us discuss the generation processes of TiO_2 particles at first. Fig. 7a shows the current density–time and voltage–time curves measured during the plasma electrolysis in $Ti(SO_4)_2$ solution with 0.3 mol L^{-1}. In order to clearly illustrate the formation of TiO_2 particles, the processes of plasma electrolysis are divided into three phases, process-I, process-II and process-III, according to the changes of voltage value as well as current density.[22–24] Fig. 7b presents the anode and cathode reactions. Fig. 7c and d respectively show the schematic illustrations and the macro states of the cathode material, corresponding with the three processes in Fig. 7a.

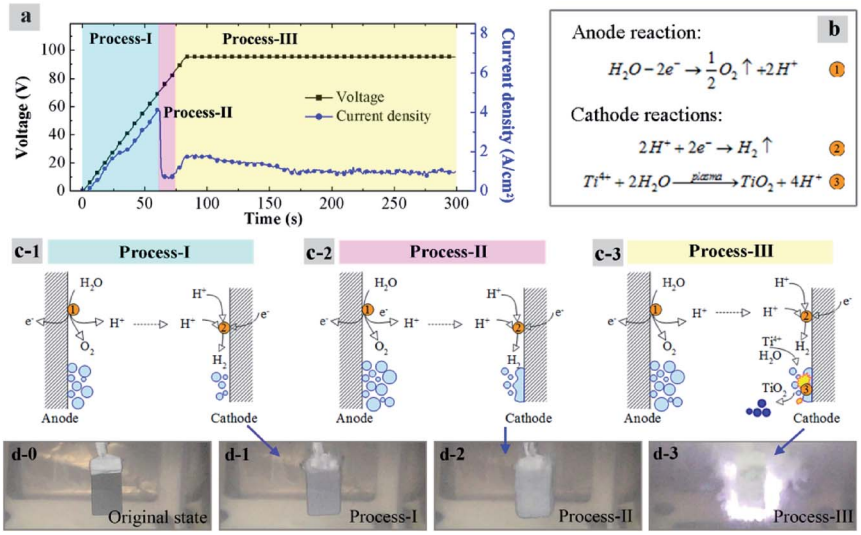

Fig. 7 Schematic illustration of plasma electrolysis processes in 0.3 mol L^{-1} $Ti(SO_4)_2$: (a) voltage–time and current density–time curves; (b) anode and cathode reactions; (c) mechanism models and (d) macro states of the cathode material in different processes.

In previous researches[22–24] it was considered that the necessary conditions for plasma discharge in the plasma electrolysis processes are the two points: first, a gas sheath must be formed on the cathode surface; second, electric field strength E of the gas sheath must reach its breakdown point.

In process-I, the voltage increases at a rate of 1 V per second. Current density increases linearly with the voltage at this initial stage. Reaction ① is taken place on the anode surface. Lots of O_2 bubbles are generated, and production of H^+ migrates to the surface of cathode. Meanwhile, H_2 bubbles are produced on the cathode surface like reaction ② in Fig. 7b. When it generates 1 mol O_2 on the anode, there will be 2 mol H_2 produced on the cathode. In addition, surface area of the cathode is much smaller than the anode. So a gas sheath will be firstly formed on the cathode surface. Once the gas sheath is formed, the current density reaches its peak-value and then decreases immediately, as shown in process-II in Fig. 7c. Plasma arc has not been formed in this phase yet, because the electric field strength E is not high enough.

When the breakdown point is reached, about 80 V as shown in process-III in this study, the plasma arc starts to be formed, as shown in Fig. 7d-3. In order to ensure the sustained and stable reactions, the actual voltage is set above the arc voltage about 15 V. So the voltage is remained at 95 V for the synthesis of particles in this experiment. Under this condition, Ti^{4+} ions on or near the cathode surface are transformed into TiO_2 with the effects of the plasma arcs, by reaction ③. Finally, particles are formed under the effect of the surface tension in the solution, shown in process-III, Fig. 7c. According to the above analysis, it is worth mentioning that this mechanism would be also applicable to the preparation of TiO_2 particles in other types of Ti^{4+} salts solutions, owing to that the SO_4^{2+} anions are considered not to participate in the reactions.

Then, how does the salt concentration affect the morphology and microstructures of the TiO_2 particles? As described in the section of Results, the morphology and phase structure of the TiO_2 particles are related to concentrations of $Ti(SO_4)_2$ solutions. The SEM and AFM results show that the surface of the particles prepared in low concentrations is rough and composed of tiny structures, while the surface of the particles prepared in higher concentrations is very smooth. The XRD and TEM results indicate that with the increase of the concentrations, the main phase of the TiO_2 particles is transformed from anatase to rutile and the grain size becomes big. To explain these phenomena and illustrate the difference among plasma energy in the $Ti(SO_4)_2$ solutions with different concentrations, the current density (i_c)–time (t) curves during the plasma electrolysis are measured and shown in Fig. 8. As analyzed in Fig. 7a, the i_c–t curves consist of three phases. TiO_2 particles are mainly formed in the last phase (generally after 100 s).

By comparing the curves in Fig. 8, we can see that the i_c in solutions with high concentrations is larger in the same process, which results in more intense energy of plasma and more violent cathode reactions in the solution with higher concentrations. When the concentration is lower than 0.3 mol L^{-1}, the current density–time curves are relatively stable, as shown in the inset in Fig. 8. At the concentration of 0.1 mol L^{-1}, the current density is about 0.50 A cm^{-2}. At 0.2 mol L^{-1}, the current density is in the range of 0.60–0.70 A cm^{-2}, and at 0.3 mol L^{-1}, the current density in the range of 0.80–1.00 A cm^{-2}. When the concentration is higher than 0.4 mol L^{-1}, the current density changes violently in the range of 0.85–1.30 A cm^{-2}. Earlier studies[7,8] have reported that the transformation temperature from anatase to rutile is in the range of 700–900 °C. It means that when the supplied energy is high enough, anatase-TiO_2 can be transformed into rutile-TiO_2. Combining the results of current density–time curves (Fig. 8) and the XRD spectrum (Fig. 4), we can draw the following conclusions. In the $Ti(SO_4)_2$ solution with low concentrations, the current density is so small that the energy for the reactions is weak, leading to the products mainly

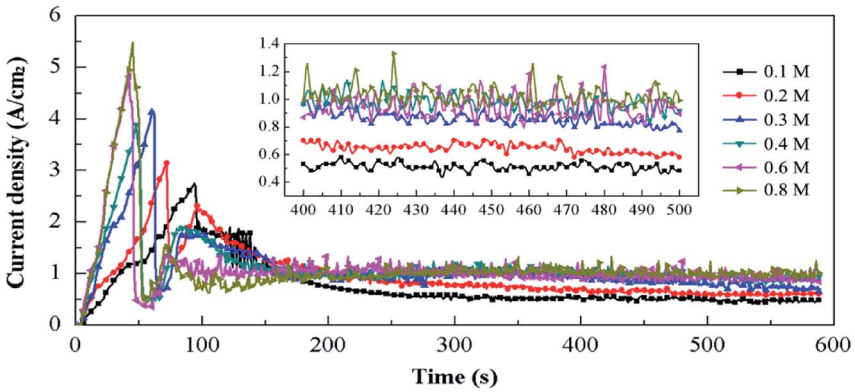

Fig. 8 Cathode current density–time curves in $Ti(SO_4)_2$ solutions with different concentrations and detail information of the curves in 400–500 s (inset).

consisting of anatase-TiO_2. When the $Ti(SO_4)_2$ concentration is high, the current density gets big. Thus, the huge energy results in high content of the rutile-TiO_2 and large size of the two kinds of grains in 0.6 mol L^{-1} and 0.8 mol L^{-1} $Ti(SO_4)_2$ solutions.

The difference of the particles' morphologies can be also explained by the current density–time curves. In the $Ti(SO_4)_2$ solutions with high concentrations, the current density is big and the cathode reactions are very fierce. Under the huge energy of the plasma, particles get smaller because of the bombardment. Meanwhile, the nano-structures existing on the surface of TiO_2 particles prepared at low concentrations disappear (Fig. 3) and the agglomeration becomes more serious (Fig. 2e and f), owing to the high temperature and melting effect. Under these conditions, products prepared in high concentrations own small particle sizes, but there are no nano-structures on their surfaces anymore.

At last, we need to clarify the function of cathode materials in the preparation of TiO_2 particles.[26–32] The compositions and micrographs of the cathode material before and after plasma electrolysis are shown in Fig. 9. XRD patterns of the initial cathode material consist of Ti (PDF-#44-1294). After the plasma electrolysis in 0.3 mol L^{-1} $Ti(SO_4)_2$ for 10 min, XRD patterns of the cathode consist of TiO_2, TiO and Ti, as shown in Fig. 9a. The results indicate that the cathode material involves in the reaction under the action of plasma. The generation of TiO_2 on cathode surface may be in connection with $Ti(SO_4)_2$ solution and TiO_2 particles. The peaks of Ti show the composition of the substrate. What's more, TiO is considered to be generated from neutral reaction of TiO_2 and Ti under high energy of plasma.

Fig. 9b and c show SEM micrographs of the cathode material before and after plasma electrolysis, respectively. Before the plasma electrolysis, the surface of cathode material is smooth, as shown in Fig. 9b. After the plasma electrolysis process, the cathode material is rough and porous (Fig. 9c), like solidified lava. The plasma discharge process of plasma electrolysis is considered to roughen the cathode surface. The diameter of the pores is about 1–3 μm, a little larger than the particle size of the product synthesized in 0.3 mol L^{-1} $Ti(SO_4)_2$ for 10 min (Fig. 2c). To confirm whether a coating is formed on the cathode surface or not, the cathode after the plasma electrolysis was further inspected under SEM for a section-cut by focused ion beam (FIB), as shown in Fig. 9d. With the aid of FIB, a trench with the depth of 5 μm can be exposed on the surface of the cathode. It is clear that there is no obvious interface and no coating in Fig. 9d. Moreover, the weights of the cathode material before and after plasma electrolysis in 0.3 mol L^{-1} $Ti(SO_4)_2$ for 10 min were measured and compared. The weight change of cathode material was in the range of ±2 mg, while the yield of the TiO_2 particles was larger than 3000 mg. These results imply that although the surface micrograph of cathode material has a significant change, the cathode is neither consumed nor coated during the TiO_2 preparation process. This is different from the processes of Al_2O_3 and $La_2Zr_2O_7$ microspheres

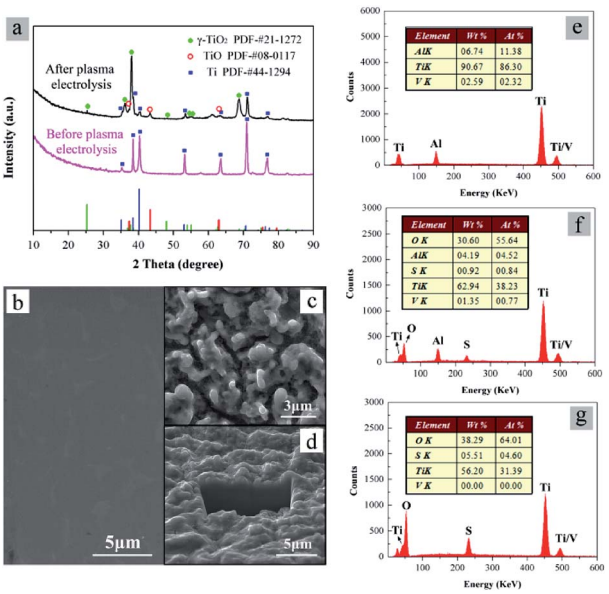

Fig. 9 (a) XRD patterns of cathode material before and after plasma electrolysis processes in 0.3 mol L^{-1} $Ti(SO_4)_2$ for 10 min; (b) and (c) SEM micrographs of cathode material before and after the plasma electrolysis; (d) SEM-FIB micrograph of the cathode material after the plasma electrolysis; (e–g) EDS analysis of cathode material before, after the plasma electrolysis and TiO_2 particles prepared in 0.3 mol L^{-1} $Ti(SO_4)_2$.

preparation[31,32] as well as the other "melting-quenching" process of the cathode material.[26–30]

In addition, the element compositions of the cathode material and TiO_2 particles are also compared with each other. Fig. 9e–g show EDS analysis of the cathode material before and after plasma electrolysis, and the TiO_2 particles prepared in 0.3 mol L^{-1} $Ti(SO_4)_2$. In Fig. 9e, there only exist elements of Ti, Al and V, conforming to the compositions of the substrate (Ti alloy). In Fig. 9f, the result shows that elementary composition of the cathode material after reactions mainly contains Ti and O, with a small amount of S, Al and V. The element of S may come from the side reaction of SO_4^{2-}. The elements of Al and V are from Ti alloy substrate. Compared with Fig. 9f, there are almost no Al and V in Fig. 9g, showing the compositions of the cathode material after reactions and the TiO_2 particles are different.

The results support again that the generation of TiO_2 particles mainly occurs at the interface of the solution and the substrate, neither on the cathode surface nor in the solution. The main source of TiO_2 particles product is Ti^{4+} in $Ti(SO_4)_2$ solution, instead of the cathode material. Under this condition, the $Ti(SO_4)_2$ concentrations instead of other parameters show the most important effect on the current density–time curves, as well as the phase and morphology of the TiO_2 particles. This is also the biggest difference with the other plasma electrolysis.[26–30]

5. Conclusions

By using a novel plasma electrolysis method, TiO_2 particles were prepared directly in aqueous solution at room temperature. The experiments found that concentration of $Ti(SO_4)_2$ solution played a very important role in the phases and morphologies of the particles. When $Ti(SO_4)_2$ concentration was in range of 0.1–0.3 mol L^{-1}, TiO_2 particles with anatase as main phase were obtained. Average grain size of the particles was about 4.0–6.0 nm and surface of the particles prepared in low concentration was rough and composed of tiny structures (about 10 nm). With increase of the concentration, the main phase of the TiO_2 particles was transformed from anatase to rutile and the grain size became big, while the particle size became small and the surface of the particles changed into smooth. When concentration was higher than 0.6 mol L^{-1}, TiO_2 particles with rutile as the main phase were prepared. Average grain size of the anatase increased to 30.0–50.0 nm, and the rutile was about 60.0–75.0 nm. Thus, by adjusting $Ti(SO_4)_2$ concentrations, phases and morphologies of the particles could be well controlled.

The formation mechanism of the TiO_2 particles, which is different from the others reported before, has been proposed, based on analyzing the current density–time curves during the plasma electrolysis, the compositions as well as microstructure of the cathode material. We can conclude that the generation of particles mainly occurred at the interface of solution and cathode substrate, and the source of the TiO_2 particles is $Ti(SO_4)_2$ instead of cathode material. Thus, the $Ti(SO_4)_2$ concentrations have a significant influence on the current density–time curves, as well as the phase and morphology of the TiO_2 particles.

Conflicts of interest

There are no conflicts to declare.

Acknowledgements

This work has been financially supported by the Chinese National Key R&D Plan (Grant No. 2016YFE0130300). The authors thank Xiaoming Xu and Wei Miao for the XRD data analysis, Huili Ren for the TEM analysis, Wenyan Yang and Rong Wang for the SEM micrographs and Weiqi Wang for the AFM measurements.

Notes and references

1 X. Chen and S. S. Mao, *Chem. Rev.*, 2007, **107**, 2891–2959.
2 U. Diebold, *Surf. Sci. Rep.*, 2003, **48**, 53–229.
3 T. K. Yun, S. S. Park, D. Kim, Y.-K. Hwang, S. Huh, J. Y. Bae and Y. S. Won, *J. Power Sources*, 2011, **196**, 3678–3682.
4 J.-H. Park, S. J. Kang, S.-I. Na, H. H. Lee, S.-W. Kim, H. Hosono and H.-K. Kim, *Sol. Energy Mater. Sol. Cells*, 2011, **95**, 2178–2185.
5 W.-Q. Wu, B.-X. Lei, H.-S. Rao, Y.-F. Xu, Y.-F. Wang, C.-Y. Su and D.-B. Kuang, *Sci. Rep.*, 2013, **3**, 1352.
6 K. S. Yeo, S. Nakao, Y. Hirose, T. Hasegawa and Y. Matsuo, *Org. Electron.*, 2013, **14**, 1715–1719.
7 K. Zakrzewska and M. Radecka, *Nanoscale Res. Lett.*, 2017, **12**, 89.
8 B. Grzmil, M. Gleń, B. Kic and K. Lubkowski, *Pol. J. Chem. Technol.*, 2013, **15**, 73–80.
9 L. Bian, M. Song, T. Zhou, J. Xu and L. Wang, *Asian J. Chem.*, 2012, **24**, 2467.
10 H. Qiao, Q. Luo, Q. Wei, Y. Cai and F. Huang, *Ionics*, 2012, **18**, 667–672.
11 R. Gao, Z. Jiao, Y. Wang, L. Xu, S. Xia and H. Zhang, *Chem. Eng. J.*, 2016, **304**, 156–164.
12 Y. V. Kolen'ko, A. A. Burukhin, B. R. Churagulov and N. N. Oleynikov, *Mater. Lett.*, 2003, **57**, 1124–1129.
13 H. Li, B. Liu, Y. Wang, S. Yin, X. Ma, X. Wang, Q. Wu, R. Shen and H. Chen, *RSC Adv.*, 2014, **4**, 37992–37997.
14 H. Li, B. Xu and Y. Fan, *Chem. Phys. Lett.*, 2013, **558**, 66–71.
15 J. Zhang, B. Wu, L. Huang, P. Liu, X. Wang, Z. Lu, G. Xu, E. Zhang, H. Wang, Z. Kong, J. Xi and Z. Ji, *J. Alloys Compd.*, 2016, **661**, 441–447.
16 J. Zhao, W. Li, X. Li and X. Zhang, *RSC Adv.*, 2017, **7**, 21547–21555.
17 Q. Zhang, X. Yan, R. Shao, H. Dai and S. Li, *J. Wuhan Univ. Technol.*, 2013, **29**, 407–409.
18 P. Billik and G. Plesch, *Mater. Lett.*, 2007, **61**, 1183–1186.
19 P. Billik, G. Plesch, V. Brezová, L. Kuchta, M. Valko and M. Mazúr, *J. Phys. Chem. Solids*, 2007, **68**, 1112–1116.
20 H. Choi, S. Khan, J. Choi, D. T. T. Dinh, S. Y. Lee, U. Paik, S.-H. Cho and S. Kim, *Appl. Catal., B*, 2017, **210**, 513–521.
21 D. Verhovšek, M. Lešnik, N. Veronovski and Z. SamardŽija, *Acta Chim. Slov.*, 2014, **61**, 468.
22 C. Liu, J. Zhang, Y. He, S. Zhang, P. Wang, Y. Lian and S. Deng, *Mater. Res. Express*, 2017, **4**, 036306.

23 A. L. Yerokhin, X. Nie, A. Leyland, A. Matthews and S. J. Dowey, *Surf. Coat. Technol.*, 1999, **122**, 73–93.
24 P. Wang, S. Deng, Y. He, C. Liu and J. Zhang, *Ceram. Int.*, 2016, **42**, 8229–8233.
25 P. Gupta, G. Tenhundfeld, E. O. Daigle and D. Ryabkov, *Surf. Coat. Technol.*, 2007, **201**, 8746–8760.
26 Z. Li, Z. Zhang and D. Guo, *Acta Phys.-Chim. Sin.*, 2010, **26**, 3106–3112.
27 Z. Zhang, M. Bai, D. Guo, S. Hou and G. Zhang, *Chem. Commun.*, 2011, **47**, 8439.
28 A. Allagui, E. A. Baranova and R. Wüthrich, *Electrochim. Acta*, 2013, **93**, 137–142.
29 A. Allagui and R. Wüthrich, *Electrochim. Acta*, 2011, **58**, 12–18.
30 G. Saito, W. O. S. B. W. M. Azman, Y. Nakasugi and T. Akiyama, *Adv. Powder Technol.*, 2014, **25**, 1038–1042.
31 C. Liu, J. Zhang, Y. He, P. Wang, S. Deng and S. Zhang, *Aust. J. Chem.*, 2017, **70**, 120.
32 C. Liu, J. Zhang, S. Deng, P. Wang and Y. He, *J. Colloid Interface Sci.*, 2016, **474**, 146–150.